Effect of Typhoon Songda (2004) on Remote Heavy Rainfall in Japan

Yongqing Wang[1,2], Yuqing Wang[2,1*], and Hironori Fudeyasu[2]

[1]Pacific Typhoon Research Center, KLME, Nanjing University of Information Science & Technology, Nanjing, China
[2]International Pacific Research Center and Department of Meteorology, University of Hawaii at Manoa, Honolulu, Hawaii

May 20, 2009
Dateline

Revised for ***Monthly Weather Review***

* Corresponding author: Dr. Yuqing Wang, IPRC/SOEST, POST Bldg. 409G, University of Hawaii at Manoa, 1680 East-West Road, Honolulu, HI 96822. E-mail:yuqing@hawaii.edu

Abstract

When Typhoon Songda (2004) was located southeast of Okinawa over the western North Pacific during 2 to 4 September 2004, a heavy rainfall event occurred in the southern central Japan and its adjacent seas, more than 1,200 km from the typhoon center. The Advanced Weather Research and Forecast (WRF_ARW) model was used to investigate the possible remote effect of Typhoon Songda on the heavy precipitation event in Japan. The National Centers for Environmental Prediction (NCEP) global final (FNL) analysis was used to provide both the initial and lateral boundary conditions for the WRF model. The model was initialized at 18 UTC 2 September and integrated until 18 UTC 6 September 2004 during which Songda was a super typhoon. Two primary numerical experiments were performed. In the control experiment, a bogus vortex was inserted into the FNL analysis to enhance the initial storm intensity such that the model typhoon had an intensity similar to the observed at the initial time. In the no-typhoon experiment, the vortex associated with Typhoon Songda in the FNL analysis was removed by a smoothing algorithm such that the typhoon signal did not appear at the initial time. As verified against various observations, the control experiment captured reasonably well the evolution of the storm and the spatial distribution and evolution of precipitation, whereas the remote precipitation in Japan was largely suppressed in the no-typhoon experiment, indicting a significant far-reaching effect of Typhoon Songda. Songda enhanced the remote precipitation in Japan mainly through the northward moisture transport into the pre-conditioned precipitation region by its outer circulation. The orographic forcing of the central mountains in Japan played a little role compared with Typhoon Songda in this extreme precipitation event studied.

1. Introduction

Tropical cyclones (TCs, or typhoons in the western North Pacific, hurricanes in the Atlantic or eastern North Pacific) are often heavy rain producers. In particular, landfalling TCs usually cause fatalities and economic losses due to not only strong winds but also torrential rainfall that often induces flash flooding after their landfall (e.g., Kunkel, et al. 1999). A TC can produce tremendous rainfall in its eyewall and both inner and outer spiral rainbands, which may be several tens to hundred kilometers from the TC center (Takahashi 1998 Lonfat et al. 2007; Kimball 2008; Yokoyama and Takayabu 2008). This is generally referred to as direct effect of a TC on precipitation, or precipitation induced by the TC itself. On the other hand, when a strong interaction with other synoptic systems occurs, a TC can induce heavy rainfall far away, for example, beyond a thousand kilometers from its center. Such an effect of a TC on precipitation in a remote area is generally referred to as indirect or remote effect of a TC on precipitation (Bosart and Carr 1978; Ross and Kurihara 1995; Chen et al. 2006).

Although most of TCs mainly produce heavy rainfall directly by themselves (direct effect), some TCs can induce heavy rainfall in remote areas when they interact with other synoptic systems, such as upper-level trough and cold frontal systems in the mid-latitudes (indirect effect). This latter, though not occurring too often, usually causes an even greater disaster when it happens because special attention is mostly given to precipitation directly caused by the TC itself (Chen et al. 2006). Quantitative precipitation forecast (QPF) is very important whereas it is quite challenging to operational forecasters. Current skill in QPF, including the forecast of TC precipitation (Elsberry 2002), is quite low. In particular, the forecast skill for TC precipitation is

largely affected by the prediction accuracy of the TC track (Chen et al. 2006; Marchok et al. 2007).

Previous studies have mostly focused on precipitation directly caused by a TC either over the open ocean (e.g., Wang and Holland 1996a, b; Rogers et al. 2003; Atallah et al. 2007) or approaching/making landfall (e.g., Li et al. 2007; Kimball 2008; Chen et al. 2006). These studies have shown that over the open ocean, the rainfall distribution in a TC is largely controlled by vertical shear in the large-scale environmental flow and the translation speed of the storm itself; while after landfall, both the rainfall intensity and the radial extent of outer rainfall are also affected by soil moisture of the underlying land surface.

Some studies have also investigated the indirect effect of a TC on remote precipitation. Bosart and Carr (1978) were among the first to document a case study for an excessive rainfall event due to the indirect effect of Hurricane Agnes (1972). They showed that a weak short wave in the mid-upper troposphere provided the initial triggering mechanism for the growth of the rain area while Agnes circulation transported plentiful moisture from the western Atlantic to the rain area, enhancing the rainfall greatly. Murata (Chen et al. 2006) studied Typhoon Meari (2004) case. Typhoon Meari made landfall in Kyushu in Japan and resulting in heavy rainfall in Kii Peninsula, more than 500 km to the east from the typhoon center. He performed a series of sensitivity numerical experiments and demonstrated that moisture supply by the typhoon outer circulation and the interaction with topography played critical roles in the heavy rainfall. Farfán and Fogel (2007) investigated the influence of eastern Pacific TC circulations on the distribution of humidity and convection over northwest Mexico. They suggested that TC activities serve as a source of

humid tropical airmasses, providing conditions to support deep convection, and thus cause heavy rainfall over northwest Mexico. Another category of the indirect effect is the downstream impact of TCs that experience extratropical transition. As recently demonstrated by Harr et al. (2008), a recurving TC undergoing extratropical transition over the Northwest Pacific could perturb the upper-level westerly jet stream in the midlatitude, exciting Rossby waves in the westerlies and impacting the midlatitude circulation and weather far downstream over the North America.

One more category of the indirect effect of a TC on remote precipitation is the remote heavy rainfall resulting from the interaction between a TC over the open ocean and a weather system (such as a cold frontal system) far away from the TC center. This type of remote effect from a typhoon over the Northwest Pacific on circulation and precipitation in Japan was previously studied by Kawamura and Ogasawara (2006) and Yamada and Kawamura (2007) with the use of reanalysis data. They found that one or two typhoons, which might serve as synoptic convective heating sources over the Northwest Pacific, could induce the quasi-stationary barotropic Rossby wavetrain emanating northeastward and significantly affect anomalous weather in the vicinity of Japan. This teleconnection was called the Pacific-Japan (PJ) pattern. They suggested that the establishment of the PJ pattern intensifies the east-west pressure gradient at low levels between a typhoon and an anomalous anticyclone east of Japan, which enhances the warm advection and moisture supply from low latitude to the vicinity of Japan, thus causing remote precipitation in Japan.

A case study for a similar scenario of the indirect effect of a typhoon on remote precipitation in Japan is investigated numerically here. The case chosen in our study was Typhoon Songda

(2004), which caused heavy rainfall in southern central Japan and adjacent seas when it was far away from the heavy precipitation region. The Advanced Research Weather Research and Forecast (WRF) model developed at the National Center for Atmospheric Research (NCAR) is used to perform two major simulations, one with and one without the typhoon circulation, to highlight the effect of Typhoon Songda (2004) on remote precipitation and to investigate the involved physical mechanisms. Several supplementary experiments are performed to examine the potential effects of topography over Japan and the radial wind profile of the typhoon itself on the simulated remote precipitation.

The rest of the paper is organized as follows. The next section provides a brief overview of Typhoon Songda (2004) and its possible contribution to the heavy rainfall in Japan. Section 3 describes the basic features of the WRF model, experimental design, including methodologies to enhance the initial typhoon vortex or remove the typhoon from the initial conditions. Results from the control simulation are verified with various available datasets in section 4. The effect of Typhoon Songda on remote precipitation in Japan and the involved physical mechanisms are discussed in section 5. Major findings are summarized in section 6.

2. An Overview of Typhoon Songda

Typhoon Songda (2004) was one of the ten named typhoons that made landfall on the main islands of Japan in 2004 and brought extensive damages to Japan due to both strong winds and heavy rainfall (Nakazawa and Rajendran 2007). It formed near the Marshall Islands on 27 August 2004 and moved northwestward over the western North Pacific. After passing the Okinawa

Islands, it recurved northeastward over the East China Sea on 12 UTC 6 September and then made landfall on Kyushu Island, south of the main island of Japan, at 00 UTC 7 September (Fig. 1). Songda reached its lifetime peak intensity with the maximum sustained near surface wind speed of 64 m s^{-1} and the minimum central sea level pressure of 916 hPa.

Similar to many other typhoons, Songda produced heavy rainfall along its track under its eyewall and in its major spiral rainbands (Fig. 1). When Typhoon Songda was located more than 1500 km south of the main islands of Japan over the western North Pacific during 18 UTC 2 through 00 UTC 5 September, a rainband with several strong convective cores occurred to the southern central Japan and the adjacent sea (135°E-145°E, 32°N -38°N, the black box in Fig. 1). It is our hypothesis that in addition to the heavy rainfall directly associated with deep convection in the inner core, Typhoon Songda contributed significantly to the heavy rainfall in the southern central Japan and the adjacent sea because its outer circulation to the east transported moisture northward to the pre-conditioned local precipitation system. This can be considered as the indirect effect of Typhoon Songda on precipitation in a remote area as discussed in section 1. Although topography in the central Japan might play a role in enhancing the heavy precipitation in Japan, the numerical results in section 5 demonstrate that the orographic effect is insignificant in the Songda case.

Figure 2 shows the synoptic patterns on 18 UTC 2 September and 00 UTC 5 September 2004 at 500 and 850 hPa. Typhoon Songda was located south of the east-west elongated subtropical ridge and embedded in the southeasterly flow on the southwestern edge of the western Pacific subtropical anticyclone at 18 UTC 2 September (Figs. 2a and 2c). To the north in the midlatitudes

was a short wave trough embedded in the westerly jet stream at 500 hPa over the Japan Sea. In addition to the main subtropical anticyclone to the east around latitude 30^{o}N, there was a subtropical anticyclonic cell at both 500 and 850 hPa over the southeastern China (Figs. 2a and 2c). This gave rise to a northeast-southwest elongated region with considerable cyclonic shear and low-level convergence between the two anticyclonic circulations over the main islands of Japan. This situation favored the upward motion and moisture convergence and served as a triggering mechanism for precipitation in the region in the coming 2-3 days (see further discussion below). By 00 UTC 5 September, the short wave trough in the westerlies moved eastward out of the domain and the jet stream in the mid-latitude weakened considerably with the development of a pair of short wave trough and ridge further to the north of Japan Sea at 500 hPa (Fig. 2b). In the lower troposphere, the cyclonic shear with horizontal wind convergence was still over Japan but weakened considerably and now Typhoon Songda was approaching the main islands of Japan from the southwest (Fig. 2d).

Accompanied with the large-scale circulation given in Fig. 2 was a northeast-southwest elongated region with cyclonic shear at the surface off the southeast coast of the main islands of Japan (Fig. 3a) and a short wave trough further to the north over Japan Sea. The short wave trough moved eastward in the following 12 h and arrived at the eastern coast of northern Japan and the cyclonic shear line moved to the southeast (Fig. 3b). In the next 12 h, the short wave trough moved eastward slowly, whereas the cyclonic shear line shifted northwestward to the southern Japan and aligned with the short wave trough to the north by 18 UTC 3 September (Fig. 3c). Corresponding to the surface wind fields was a northeast-southwest elongated cyclonic vorticity

zone in the lower troposphere over the southern central Japan at 18 UTC 2 (Fig. 3d) with the development of low-level convergence by 06 UTC 3 September (Fig. 3e). By 18 UTC 3, a strong convergence zone at 850 hPa with upward motion (not shown) developed over the southern central Japan and the adjacent seas. This is the time when significant rainfall started in the region. Therefore, the low-level cyclonic shear zone with strong horizontal wind convergence was the key to the vertical motion and thus the pre-conditioning and initiation of precipitation over the southern central Japan and the adjacent seas, where the troposphere was already conditionally unstable to cumulus convection (not shown). We will show in section 5 that the northward moisture transport by the low-level southerly-southeasterly flow of the Songda's outer circulation was crucial to the subsequent heavy rainfall over Japan.

Figure 4 shows the satellite images over the East Asia and western North Pacific. There were two major cloud systems in the region: one to the southeast of Okinawa Islands associated with Typhoon Songda and the other associated with the surface shear line across the main islands of Japan during 12 UTC 3 September and 06 UTC 4 September. Although interactions might exist between the two cloud systems, they were definitely separate systems during this period. After 00 UTC 5 September, Typhoon Songda headed northeastward, approaching the main islands of Japan, and followed by the direct effect of the typhoon itself on precipitation in Japan. Since the focus of this study is on the indirect effect of Typhoon Songda on precipitation in Japan, our attention would thus be given to the period during 18 UTC 2 September through 00 UTC 5 September 2004.

3. Model configuration and experimental design

a. Model configuration

The model used in this study is the Version 2.2.1 of the Advanced Research WRF ARW model developed at NCAR (Skamarock et al. 2008). WRF ARW is a three-dimensional, fully-compressible, non-hydrostatic model formulated in a terrain-following mass coordinate in the vertical. The model physics include the grid-scale cloud and precipitation scheme used in the new Eta model, namely, the Ferrier cloud microphysics scheme (Ferrier 1994), the Rapid Radiative Transfer Model (RRTM) for longwave radiation (Mlawer et al. 1997), the Goddard shortwave radiation scheme (Chou and Suarez 1994), the Monin-Obukhov surface flux calculation over the ocean, the RUC land-surface model (Smirnova et al. 1997, 2000), the Yonsei University (YSU) planetary boundary layer scheme (Hong et al. 2006), and Kain-Fritsch cumulus parameterization scheme (Kain and Fritsch 1990) for subgrid scale deep convection.

Three interactive nesting domains (Fig. 1) are used in all numerical experiments performed in this study. The outermost domain (D1) had 166 × 166 grid points, centered at 30°N, 135°E, with the horizontal grid spacing of 27 km. The second domain (D2) had 370 × 370 grid points with the horizontal grid spacing of 9 km. The innermost domain (D3) had 673 × 379 grid points with the horizontal grid spacing of 3 km, which covers the precipitation region in Japan and the adjacent seas. The second domain D2 was used to explicitly resolve the structure of the typhoon and the mesoscale precipitation systems as was briefly discussed in section 2 above. The innermost domain D3 was used to better resolve the fine structure of the frontal system near Japan. Note that the cumulus parameterization was not activated in domain D3. The model was run with 28

unevenly distributed vertical levels with higher resolution in the planetary boundary layer and with the model top at 10 hPa. The NCAR-archived NCEP (National Centers for Environmental Prediction) global final (FNL) analysis dataset at 1° by 1° longitude/latitude grids and 6-h intervals was used to provide both the initial and lateral boundary conditions to the WRF ARW model. Sea surface temperature (SST) used in the model simulation was from the NCEP real time objective SST analysis with a 0.5° by 0.5° horizontal grid spacing at the initial time and did not change during the model simulation. This could be a limitation for the realistic simulation of the typhoon intensity.

b. Experimental design

Four numerical experiments were performed using the model configuration above in this study. The control experiment (CNTRL) was designed to reproduce the observed nature discussed in section 2. Typhoon Songda (2004) from the FNL analysis (Fig. 5a) was too weak compared with the best track and observations partly due to the sparse conventional observations over the open ocean and partly due to the coarse resolution global model used in the data assimilation for the FNL analysis. Indeed, we could not expect the FNL analysis to depict the maximum inner core intensity of a typhoon because its coarse resolution and its representative of the grid box mean quantities. Therefore, in order to realistically represent the typhoon in the simulation, the initial model typhoon needs to be enhanced in some way to match the observed intensity and structure. Although different methods could be used to achieve this, such as bogus data assimilation (DBA, e.g., Zou and Xiao 2000; Xiao et al. 2000), we chose a simple bogus scheme in this study (Wang 1998). Following Wang (1998), the tangential flow (V_T) of the bogus vortex is defined by

$$V_T(r,\sigma) = V_m(\frac{r}{r_m})\exp[1-(\frac{r}{r_m})]\sin(\frac{\pi}{2}\sigma) \quad (1)$$

where r denotes radial distance from the observed typhoon center, and V_m (55 m/s) is the maximum azimuthal wind at the radius of r_m (60 km), $\sigma = (p-p_t)/(p_s-p_t)$ with p the pressure and p_s and p_t being unperturbed pressure at the sea surface and at p=100 hPa, respectively. Geopotential height was calculated by gradient wind balance on constant pressure surfaces and the temperature anomaly was obtained from thermal wind balance. This axisymmetric vortex was inserted into the FNL analysis fields without any other special treatment, which seemed to work well for this case.

After inserting the bogus vortex into the initial analysis, the initial model typhoon (Fig. 5b) was much stronger than that in the FNL analysis (Fig. 5a). The initial maximum wind on 1000 hPa pressure level was increased from 20 m s^{-1} in the FNL analysis to 53 m s^{-1} (not shown), which is very close to 56 m s^{-1} of the Joint Typhoon Warning Center (JTWC) best track at the given time. The minimum sea level pressure was decreased from 991 hPa in the FNL analysis to 934 hPa (not shown), which is about 7 hPa higher than that given in the JTWC best track. The bogus vortex scheme enhances the inner core structure and intensity of the initial typhoon vortex but has little effect beyond about 300 km in the FNL analysis (Fig. 6). Therefore, the initial field in the control experiment improved the representation of the typhoon vortex considerably and is suitable for this study because we mainly focus on the effect of the vortex-scale cyclonic circulation on precipitation in the remote areas.

The indirect effect of Typhoon Songda on the remote precipitation in the southern central Japan in the control experiment was isolated by conducting a sensitivity experiment

(No-Typhoon), in which the typhoon circulation was removed from the FNL analysis which provided the lateral boundary conditions to the WRF model. The typhoon vortex removal algorithm used by Ross and Kurihara (1995) was adopted in this study. In our application, the successive application of a simple smoothing operator of Kurihara et al. (1990) was applied to winds, geopotential height, temperature, and specific humidity fields of the FNL analysis centered at the observed typhoon center at a given time. Figure 5c shows the typhoon component in the FNL analysis field, and Fig. 5d shows the initial fields with the typhoon vortex removed at 850 hPa. Therefore, we can expect that the difference between the CNTRL and No-Typhoon experiments can be considered as the effect of the typhoon on its environment.

Other two sensitivity experiments were also performed. The No-Bogus experiment is the same as the CNTRL experiment but without the application of the bogus scheme described above. This experiment was designed to see whether the outer circulation of the model typhoon was artificially enhanced by the bogus scheme, thus overestimating the effect of the typhoon on the remote precipitation in Japan in the CNTRL experiment. The last experiment (No-Terrain) is the same as the CNTRL experiment but with the terrain height over the main islands of Japan set to 1 m if it is higher than 1 m so that the possible effect of topography on precipitation over Japan was artificially eliminated. This experiment was intended to address whether the interaction between the outer circulation of Typhoon Songda and the orography in central Japan played any role in the heavy precipitation over Japan.

4. Verification of the control simulation

Figure 7a compares the observed and the CNTRL experiment simulated maximum 10-m height surface wind speed and minimum sea level pressure. Overall, the model simulated reasonably well the intensity evolution of Typhoon Songda except that the simulated typhoon was stronger than the observed after about 48 h of integration (Fig. 7a) due to the considerable underestimation of the weakening of Typhoon Songda. Figure 7b shows the track of Typhoon Songda from both the observation and the model simulation. Although the anticyclonic track was reproduced well by the model, the simulated track had a systematic deflection to the left of the best track. This discrepancy in the simulated track could be attributed to either the relatively large size of the model typhoon (Wang and Holland 1996a, b), or the bias in the simulated large-scale environmental flow due to problems with model physics, or initial data, or both. Despite the bias in the simulated track, the large-scale outer circulation of Typhoon Songda is likely similar to that observed. Therefore, the effect of Typhoon Songda on precipitation in Japan should be reasonably captured by the model in this case (see next section).

Verification of the simulated typhoon structure is challenging due to the lack of observations over the open ocean. However, the inner core structure of the simulated storm can be compared with the Tropical Rainfall Measuring Mission (TRMM) Precipitation Radar (PR) observations. Owing to the narrow swath of the TRMM satellite, PR data are limited by sampling. What we did here was to pick up the model times close to the times of the PR data available to us and compared the surface rain rate from the model simulation with the PR observation.

Figure 8 shows 3 examples of such a comparison during 3-4 September 2004. The TRMM/PR data give fine structure and evolution of precipitation in the inner core region of

Typhoon Songda. In particular, Songda seemed to evolve a concentric eyewall cycle (Willoughby et al. 1982) during the given time period (left panels in Fig. 8). The model failed to reproduce the concentric eyewall cycle, however. Instead, the model simulated a relatively large eye and eyewall structure with stronger surface rain rates in the eyewall (right panels in Fig. 8). This is not surprising since the initial model typhoon did not include the detailed information of the preconditioning of the concentric eyewall development and the simulation of concentric eyewall is still a challenge task for most numerical models (e.g., Houze et al. 2007).

Although the model did not capture the inner eyewall of Typhoon Songda, it did produce the eyewall size equivalent to the size of the outer eyewall from the TRMM/PR observations. This may imply that the overall inner-core size of the model typhoon is not unrealistic compared with the real typhoon. The stronger rain rates in the simulation could be partially due to the discrepancies in the cloud microphysics scheme used in the model, or in initial conditions, or model resolution. Again, since our focus of this study is on the effect of the outer circulation of Typhoon Songda on remote precipitation far to the north in the central Japan, the lack of the concentric eyewall structure in the simulation is not expected to alter our qualitative conclusions regarding Typhoon Songda's remote effect on precipitation over Japan, which will be discussed in the next section.

Total precipitation between 18 UTC 2 September and 00 UTC 5 September 2004 in the control simulation is shown in Fig. 9a. Compared with the total precipitation during the same time period from the TRMM TMI products (Fig. 1), the control experiment simulated reasonably well the observed spatial pattern of precipitation (Fig. 9a). However, as mentioned earlier, the model

overestimated the rainfall in the inner-core region along the typhoon track. The precipitation to the north over the main islands of Japan was underestimated, however. The spatial distribution of the simulated precipitation is much smoother than observed. This may be partially due to the relatively coarse model resolution in domain 3 in this study. However, we expect that most of the discrepancies in the control simulation would not prohibit us from a qualitative assessment of the possible effect of Typhoon Songda on the remote precipitation in Japan as discussed in the next section.

5. Effect of Typhoon Songda on remote precipitation in Japan

Figure 9b shows the total precipitation from the No-Typhoon experiment during the same period as shown in Fig. 9a from the CNTRL experiment. As expected, with the typhoon removal in the No-Typhoon experiment, precipitation originally associated with Typhoon Songda over the western North Pacific almost disappeared, indicating the removal of the Typhoon Songda's direct effect on precipitation along its path. In addition to the direct effect, Songda had an indirect effect on precipitation far to the north over the main island of Japan. Comparing Figs. 9a and 9b, with the typhoon removed in the No-Typhoon experiment, precipitation over the main islands of Japan and the adjacent seas was substantially reduced, suggesting that Typhoon Songda contributed positively to precipitation in Japan (rectangular box in Fig. 9). In addition, precipitation over the North Pacific to the east of Japan and in the lower reaches of Yangtze River was increased slightly in the No-Typhoon experiment, implying that Typhoon Songda might play a role in suppressing precipitation in the two areas. This indirect effect could be related to the modification of the

large-scale flow pattern by the typhoon outer circulation. Compared to the change in precipitation over Japan and adjacent seas, the changes in other regions are modest. Therefore, our following analysis will focus on the effect of Typhoon Songda on remote precipitation over Japan and adjacent seas.

Figure 10 shows the temporal evolution of the area averaged 6-hourly rainfall in the box of 32°-38°N, 135°-145°E (rectangular box in Fig. 9) from the TRMM TMI observation, CNTRL and No-Typhoon experiments. Although the CNTRL experiment underestimated the total precipitation in the given region (Fig. 9), the underestimation occurred mainly during the period from 06 UTC 4 to 00 UTC 5 September 2004, namely, the period with heavy rainfall (Fig. 10). Nevertheless, the reduction of precipitation in the region due to the removal of typhoon is dramatic, indicating that Typhoon Songda contributed over 90% to the precipitation over Japan and adjacent seas during 12 UTC 3 to 00 UTC 5 September 2005. Note that the large-scale circulation fields, in particular the short wave trough north of 30^{o}N in the mid-lower troposphere in the CNTRL and No-Typhoon experiments are similar (Figs. 11a and 11d), indicating that the pre-conditioned mid-latitude circulation system was not substantially altered by Typhoon Songda. However, as we can see from Fig. 11, the moisture fields changed dramatically in the precipitation region over the main islands of Japan and adjacent seas south of Japan due to the removal of Typhoon Songda. To investigate how the typhoon affected the remote precipitation in Japan, we performed a diagnostic analysis on moisture transport and two additional numerical experiments (namely, No-Bogus and No-Terrain) as discussed below.

a. Moisture transport

Typhoon Songda might significantly transport warm and moist air to the north in its northeast quadrant due to the southerly winds of its outer cyclonic circulation and high moisture content in its circulation (left panels in Fig. 11). The southerly winds in the control experiment were also enhanced due to the increased pressure gradient between the typhoon and the subtropical high to the east (as suggested by Kawamura and Ogasawara 2006), contributing to a moisture convergence zone to the north in the pre-conditioned precipitation region over Japan. The vertical cross-section of the meridional moisture fluxes ($\rho q_v v$, where q_v is water vapor mixing ratio and v the meridional wind speed) along 30°N for a snapshot at 12 UTC 4 September and for an average between 18 UTC 2 and 00 UTC 5 September are shown in Fig. 12. Comparing Fig. 12 (left panels) with Fig. 10, one can see that the deep layer northward moisture transport from the CNTRL experiment contributed significantly to the precipitation in the central region of Japan. In contrast, with the typhoon removed in the No-Typhoon experiment, the southerly winds to the west of the subtropical high were much weaker than that in the CNTRL experiment, leading to a large reduction of the northward moisture transport, in particular, in the longitude band with strong precipitation in Japan.

The column-integrated moisture flux divergence is a good measure whether the northward transported moisture contributed to the precipitation (Banacos and Schultz 2005) in the CNTRL experiment. At a given time it can be expressed as

$$M = \int_0^{z_t} \nabla \cdot \left(\rho q_v \vec{V}\right) dz \qquad (2)$$

where q_v is water vapor mixing ratio, $\vec{V}$ is the horizontal wind vector, z is the height and z_t is the

height of the model top.

Figure 13 shows an example of the column-integrated moisture flux divergence at 12 UTC 4 September, namely, at the time close to the observed maximum rainfall (Fig. 10), from the CNTRL and No-Typhoon experiments, respectively. In the CNTRL experiment, the areas with large moisture convergence are collocated with the regions with heavy rainfall shown in Fig. 9a. The large moisture flux convergence exists in the inner core region of the typhoon. Also a northeast-southwest elongated moisture flux convergence belt is associated with the rainfall over the main islands of Japan. With the typhoon vortex removed in the No-Typhoon experiment, as expected, the moisture flux convergence associated with the typhoon disappeared, and the moisture flux convergence belt along the Japan main islands was largely suppressed, consistent with the largely reduced precipitation in the region as shown in Fig. 9b.

Figure 14 gives the temporal evolution of the area-averaged column-integrated moisture flux divergence from 18 UTC 2 to 18 UTC 5 September 2004 from all four experiments. Comparing Fig. 14 and Fig. 10, one can find that precipitation is well correlated with but lags the column-integrated moisture flux convergence by about 3-6 hours. Consistent with the precipitation shown in Fig. 10, the column-integrated moisture flux convergence is quite small in the No-Typhoon experiment, indicating that Typhoon Songda not only contributed to the northward moisture transport but also the moisture flux convergence in the precipitation region in Japan and the adjacent seas.

b. Effect of the bogus vortex

The indirect effect of Typhoon Songda on remote precipitation in Japan was through its

outer cyclonic circulation, which significantly enhanced the northward moisture transport and contributed to the moisture convergence in the remote precipitation region. Questions arise as to whether the effect of Typhoon Songda on remote precipitation over Japan was artificially overestimated due to the introduction of a bogus vortex used in the CNTRL experiment. To address this issue, an experiment (No-Bogus) initialized with the FNL analysis without the application of the bogus vortex scheme was conducted. Although the FNL analysis can not resolve the inner core structure of the typhoon, it can depict reasonably well the outer circulation of the typhoon since it includes observations from large-scale observational network and the assimilation of satellite data.

Although the simulated storm in the No-Bogus experiment was much weaker than that in the CNTRL experiment (Figs. 9a and 15a), precipitation over Japan and adjacent seas in the No-Bogus experiment was generally similar to that in the CNTRL experiment in both the spatial distribution in the time mean (Fig. 15a) and the temporal evolution of the area averaged rainfall (Fig. 10). This is consistent with the similar moisture flux convergence in the No-Bogus and in the CNTRL experiments as shown in Fig. 14. The overall feature of the indirect effect of the model typhoon on the remote precipitation over Japan and adjacent seas is little altered even though no bogus vortex is used in the initial conditions, indicating that the initial vortex bogus mainly improved the simulation of the inner core intensity and had little effect on the outer circulation of the storm in this case.

c. Topographic effect

Another seemingly important factor that might affect the precipitation over Japan is the

orographic lifting of warm, moist air from the southeast that could enhance precipitation on the southern slope over the mountains in the central Japan. This may be the case since precipitation over the Japan was to the south (windward side) of the mountainous areas in the central Japan (Fig. 1). To examine this possibility, a No-Terrain experiment was conducted in which the terrain height over the main island of Japan was set to 1 m if it is higher than 1 m so that the orographic effect on precipitation over Japan would be eliminated.

Total precipitation between 18 UTC 2 September and 00UTC 5 September 2004 in the No-Terrain experiment (Fig. 15b) has a spatial distribution very similar to that in the CNTRL experiment (Fig. 9a) but the precipitation amount was slightly reduced in the former. This can also be clearly seen from the temporal evolution of 6-hourly rainfall in the boxed area in Fig. 1 from the No-Terrain experiment (Fig. 10). There was no significant difference in the moisture flux divergence between the No-Terrain and CNTRL experiments (Fig. 14), indicating that the orographic lifting enhanced the precipitation over the central Japan. For the case studied, the orographic forcing contributed to precipitation over Japan by about 10% and thus it is the secondary to the overall precipitation process compared to the effect of Typhoon Songda.

6. Conclusions

The Advanced Research WRF ARW model has been used to investigate the possible effect of Typhoon Songda (2004) over the western North Pacific on precipitation in a remote area to its north over the central Japan and the involved physical mechanisms. In this case, when Typhoon Songda was located southeast of Okinawa, heavy rainfall occurred far to the north over the

southern central Japan and its adjacent seas. In a control experiment with an initial vortex enhancement algorithm, the model reasonably reproduced the major features of the observed Typhoon Songda and precipitation over Japan. To explicitly demonstrate the contribution of Typhoon Songda to the remote precipitation in Japan, a no-typhoon experiment was performed in which the typhoon vortex was removed from the NCEP FNL analysis fields that provided both the initial and lateral boundary conditions to the WRF ARW model. As a result of the removal of the model typhoon, precipitation over central Japan and the adjacent seas associated with a pre-conditional cyclonic shear, convergence zone was largely suppressed, indicating the dominant control of Typhoon Songda on the remote precipitation for the case studied.

The major process involved in the remote effect of Typhoon Songda is through the enhanced northward moisture transport into the pre-conditioned precipitation region by its outer circulation. As a result, the presence of Typhoon Songda was critical to the observed heavy rainfall in central Japan and the adjacent seas even though the typhoon was more than 1,200 km to the south over the western North Pacific. In another experiment with the terrain removed over Japan, the overall precipitation pattern was very similar to that from the control simulation except for a 10% underestimation of the precipitation, indicating that the local orographic forcing played a secondary role in the case studied.

Acknowledgments: The authors are grateful to Prof. David Schultz and Dr. Ron McTaggart-Cowan for their critical and constructive comments which helped improve the quality of this work. This study has been supported by NSF grants ATM-0427128 and ATM-0754029 and

ONR grant 000-14-06-10303. Additional support has been provided by JAMSTEC of Japan, NASA, and NOAA through their sponsorships of the International Pacific Research Center in School of Ocean and Earth Science and Technology at University of Hawaii.

References:

Atallah, E., L. F. Bosart, and A. R. Aiyyer, 2007: Precipitation distribution associated with landfalling tropical cyclones over the eastern United States. *Mon. Wea. Rev.* **135**, 2185-2206.

Banacos, P. C., and D. M. Schultz, 2005: The use of moisture flux convergence in forecasting convective initiation: Historical and operational perspectives. *Mon. Wea. Rev.*, **20**, 351-366.

Bosart, L. F., and F. H. Carr, 1978: A case study of excessive rainfall centered around Wellsville, New York, 20-21 June 1972. *Mon. Wea. Rev.*, **106**, 348-362.

Chen, L.-S., and working group members, 2006: Observations and forecast of rainfall distribution. Topic 0.3, Workshop Topic Reports of the Sixth WMO International Workshop on Tropical Cyclones (IWTC-VI), TMRP 72, 36-42.

Chou, M.-D., and M. J. Squarez, 1994: An efficient thermal infrared radiation parameterization for use in general circulation models. NASA Tech. Memo. 104606, 3, 85 pp.

Elsberry, R. L., 2002: Predicting hurricane landfall precipitation: Optimistic and pessimistic views from the symposium on precipitation extremes. *Bull. Amer. Meteor. Soc.,* **83**, 1333–1339.

Farfán, L. M., and I. Fogel, 2007: Influence of tropical cyclones on humidity patterns over Southern Baja California, Mexico. *Mon. Wea. Rev.,* **135**, 1208–1224.

Ferrier, B. S., 1994: A double-moment multiple-phase four-class bulk ice scheme. Part I: Description. *J. Atmos. Sci*., **51**, 249-280.

Harr, P. A., D. Anwender, and S. C. Jones, 2008: Predictability associated with the downstream impacts of the extratropical transition of tropical cyclones: Methodology and a case study of

Typhoon Nabi (2005). *Mon. Wea. Rev.*, **136**, 3205–3225.

Hong, S.-Y., Y. Noh, and J. Dudhia, 2006: A new vertical diffusion package with an explicit treatment of entrainment processes. *Mon. Wea. Rev.*, **134**, 2318-2341.

Houze, R. A., Jr., S. S. Chen, B. F. Smull, W.-C. Lee, and M. M. Bell, 2007: Hurricane intensity and eyewall replacement. *Science*, **315**, 1235-1239.

Kain, J. S., and J. M. Fritsch, 1990: A one-dimensional entraining/detraining plume model and its application in convective parameterization. *J. Atmos. Sci.*, **47**, 2784–2802.

Kawamura, R., and T. Ogasawara, 2006: On the role of typhoons in generating PJ teleconnection patterns over the western North Pacific in late summer. *SOLA*, **2**, 37-40, doi:10.2151/sola.2006-010.

Kimball, S. K., 2008: Structure and evolution of rainfall in numerically simulated landfalling hurricanes. *Mon. Wea. Rev.*, **136**, 3822–3847.

Kunkel, K. E., R. A. Pielke Jr., and S. A. Changnon, 1999: Temporal fluctuations in weather and climate extremes that cause economic and human health impacts: A review. *Bull. Amer. Meteor. Soc.*, **80**, 1077–1098.

Kurihara, Y., M. A. Bender, R. E. Tuleya, and R. J. Ross, 1990: Prediction experiments of hurricane Gloria (1985) using a multiply nested movable mesh model. *Mon. Wea. Rev.*, **118**, 2185–2198.

Li, Y., J.-Z. Wang, L.-S. Chen, and Y.-Q. Yang, 2007: Study on wavy distribution of rainfall associated with typhoon Masta (2005). *Chinese Sci. Bull.*, **52**, 972-983.

Lonfat, M., R. Rogers, T. Marchok, and F. D. Marks Jr, 2007: A parametric model for predicting

hurricane rainfall. *Mon. Wea. Rev.*, **135**, 3086-3096.

Marchok, T., R. Rogers, and R. Tuleya, 2007: Validation schemes for tropical cyclone quantitative precipitation forecasts: Evaluation of operational models for U.S. landfalling cases. *Wea. Forecasting,* **22**, 726–746.

Mlawer, E. J., S. J. Taubman, P. D. Brown, M. J. Iacono, and S. A. Clough, 1997: Radiative transfer for inhomogeneous atmosphere: RRTM, a validated correlated-*k* model for the long-wave. *J. Geophys. Res.*, **102** (D14), 16663-16682.

Nakazawa, T., and K. Rajendran, 2007: Relationship between tropospheric circulation over the western North Pacific and tropical cyclone approach/landfall on Japan. *J. Meteor. Soc. Japan*, **85**, 101-114.

Ross, R. J., and Y. Kurihara, 1995: A numerical study on influences of Hurricane Gloria (1985) on the environment. *Mon. Wea. Rev.*, **123**, 332-346.

Rogers, R., S. Chen, J. Tenerelli, and H. Willoughby, 2003: A numerical study of the impact of vertical shear on the distribution of rainfall in Hurricane Bonnie (1998). *Mon. Wea. Rev.* **131**, 1577–1599.

Skamarock, W. C., and co-authors, 2008: A Description of the Advanced Research WRF Version 3. NCAR Technical Note, NCAR/TN-475+STR, 113 pp.

Smirnova, T. G., J. M. Brown, and S. G. Benjamin, 1997: Performance of different soil model configurations in simulating ground surface temperature and surface fluxes. *Mon. Wea. Rev.*, **125**, 1870-1884.

Smirnova, T. G., J. M. Brown, S. G. Benjamin, and D. Kim, 2000: Parameterization of cold-season

processes in the MAPS land-surface scheme. *J. Geophys. Res*., **105** (D3), 4077-4086.

Takahashi, T., and T. Kawano, 1998: Numerical sensitivity study of rainband precipitation and evolution. *J. Atmos. Sci.* **55** 57-87.

Wang, Y., 1998: On the bogusing of tropical cyclones in numerical models: The influence of vertical structure. *Meteor. Atmos. Phys*., **65**, 153-170.

Wang Y., and G. J. Holland, 1996a: The beta drift of baroclinic vortices. Part II: Diabatic vortices. *J. Atmos. Sci*., **53**, 3737-3756.

Wang, Y., and G. J. Holland, 1996b: The beta drift of baroclinic vortices. Part I: Adiabatic vortices. *J. Atmos. Sci*., **53**, 411-427.

Willoughby, H. E., J. A. Clos, and M. G. Shoreibach, 1982: Concentric eyewalls, secondary wind maxima, and the evolution of the hurricane vortex. *J. Atmos. Sci.*, **39**, 395-411.

Xiao, Q., X. Zou, and B. Wang, 2000: Initialization and simulation of a landfalling hurricane using a variational bogus data assimilation scheme. *Mon. Wea. Rev.*, **128**, 2252–2269.

Yamada, K., and R. Kawamura, 2007: Dynamical link between typhoon activity and the PJ teleconnection pattern from early summer to autumn as revealed by the JRA-25 reanalysis. *SOLA*, **3**, 65-68, doi:10.215/sola.2007-017.

Yokoyama, C., and Y. N. Takayabu, 2008: A statistical study on rain characteristics of tropical cyclones using TRMM satellite data. *Mon. Wea. Rev.***, 136,** 3848–3862.

Zou, X., and Q. Xiao, 2000: Studies on the initialization and simulation of a mature hurricane using a variational bogus data assimilation scheme. *J. Atmos. Sci.*, **57**, 836–860.

Figure Caption

Fig. 1. Total precipitation (mm) between 18 UTC 2 and 00 UTC 5 September 2004 and the best-track of Typhoon Songda (2004) from JTWC (http://metocph.nmci.navy.mil/jtwc). The TRMM 3B42 V6 3-hourly merged rainfall dataset, which was obtained from the Asia-Pacific Data-Research Center (APDRC) at University of Hawaii, was used. The same precipitation dataset was used as observed precipitation in Fig. 10 as well. The small box in D3 shows the interested area that will be used for area average in Fig. 10.

Fig. 2. Geopotential height (10 gpm in contours) and wind (wind barbs) fields at 500 hPa (upper) and 850 hPa (lower) with contour interval of 40 gpm from the FNL analysis for 18 UTC 2 (left panels) and 00 UTC 5 September 2004 (right panels). One flag represents 50 knots and one full barb represents 10 knots.

Fig. 3. 10-m wind (wind bars in m s^{-1}) and sea level pressure (contours with interval of 1 hPa) fields (left) and the horizontal divergence (shading in 10^{-5} s^{-1}) and relative vertical vorticity (contours with interval of 0.1×10^{-4} s^{-1}) at 18 UTC 2 (a and d), 06 UTC 3 (b and e), and 18 UTC 3 (c and f) September, 2004 from FNL analysis. One flag represents 50 knots and one full barb represents 10 knots. Thick Dashed line segments in (a)-(c) show either a short wave trough in the mid-latitude westerlies or a cyclonic shear line in the surface wind fields.

Fig. 4. Satellite images over the East Asia and western North Pacific (obtained from Korean Meteorological Administration), showing the evolution of Typhoon Songda (2004) and the precipitation system over the southern central Japan and adjacent seas with the time given at the top of each panels.

Fig. 5. Geopotential height (contours in 10 gpm with contour interval of 40 gpm) and wind (wind barbs) fields at 850 hPa 18 UTC 2 September 2004. (a) The FNL analysis; (b) initial condition in the control experiment with the enhanced typhoon vortex in the FNL analysis using a bogus vortex scheme; (c) the typhoon vortex removed from the FNL analysis; and (d) The initial condition in the No-Typhoon experiment with the typhoon vortex removed. One flag represents 50 knots and one full barb represents 10 knots.

Fig. 6. Radial profiles of azimuthal mean tangential wind (m s^{-1}) at 850 hPa in the control experiment with a vortex bogus scheme (dashed) and in the No-Bogus experiment with no bogus vortex (solid) at the initial time (18 UTC 2 September 2004).

Fig. 7. (a) Evolution of the minimum central sea level pressure (hPa) and the maximum sustained 10-m wind speed (m s^{-1}); and (b) the storm track from the JTWC best track data (dashed) and the WRF model simulation in the control experiment (solid).

Fig. 8. Precipitation rates (mm h^{-1}) from the TRMM PR data (left) at 02:29:50-02:33:09 UTC 3 (top), 03:11:24-03:14:53 UTC 4 (middle), and 19:42:46-19:46:05 UTC 4 (bottom) September 2004; and from the control experiment (right) at 03 UTC 3 (top), 03 UTC 4 (middle), and 20 UTC 4 (bottom) September 2004.

Fig. 9. Total precipitation (mm) between 18 UTC 02 September and 00 UTC 05 September 2004 in (a) the control experiment and (b) the No-Typhoon experiment. The typhoon track during this time period together with the minimum central sea level pressure from the control experiment is also shown in (a). The small box in each panel shows the interested area, the same as in Fig. 1, that will be used for area mean in Figs. 10 and 14.

Fig. 10. Temporal evolution of 3-hourly rainfall (mm) from 21 UTC 2 to 18 UTC 5 September averaged in the area of 135°-145°E, 32°-38°N, namely, the box shown in Figs. 1 and 9, from the CNTRL, No-Typhoon, No-Terrain, No-Bogus experiment, and TRMM observation.

Fig. 11. Geopotential height (contours in 10 gpm with contour interval of 40 gpm), specific humidity (shading in g kg^{-1}), and wind (m s^{-1}, wind barbs) fields at 850 hPa from the control (left) and No-Typhoon (right) experiments, respectively, at 00 UTC 3 (top), 00 UTC 4 (middle), and 00 UTC 5 (bottom), September, 2004. One flag represents 50 knots and one full barb represents 10 knots.

Fig. 12. Meridional moisture flux (10^3 g m^{-2} h^{-1}) across 30°N, (a) and (b) at 12 UTC 04 September 2004, (c) and (d) averaged between 18 UTC 2 and 00 UTC 5 September 2004. (a) and (c) from the control experiment, and (b) and (d) from the No-Typhoon experiment. Contour interval is 15×10^3 g m^{-2} h^{-1} and areas with values greater than 15×10^3 g m^{-2} h^{-1} are shaded. The longitude area of 135°-145°E for the box in Figs. 1 and 9 is marked with vertical dashed lines.

Fig. 13. Column-integrated moisture flux divergence (10^3 g m^{-2} h^{-1}) at 12 UTC 4 September 2004 from (a) the control experiment and (b) the No-Typhoon experiment.

Fig. 14. The temporal evolution of the moisture flux divergence (10^3 g m^{-2} h^{-1}) averaged in the box given in Fig. 9 during 21 UTC 2 and 18 UTC 5 September 2004 from the control, No-Typhoon, No-Terrain, and No-Bogus experiments.

Fig. 15. Same as Fig. 9 but for (a) the No-Bogus experiment and (b) the No-Terrain experiment.

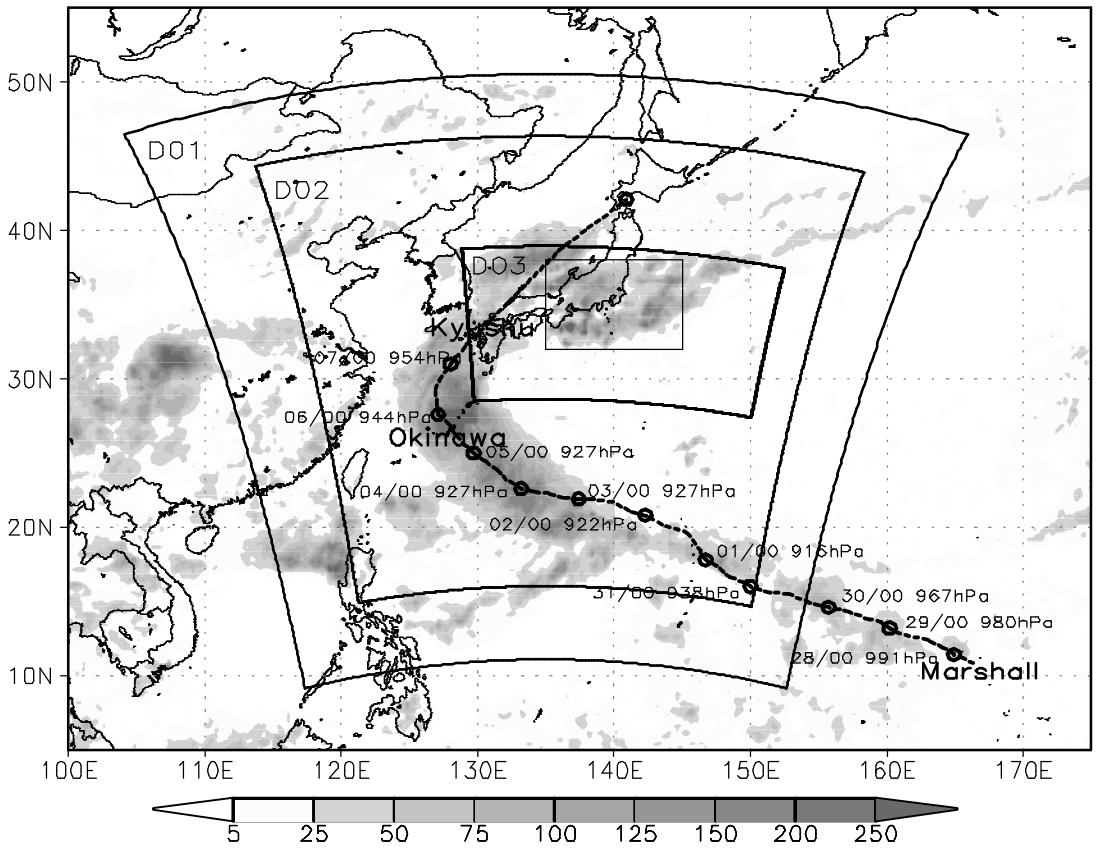

Fig. 1. Total precipitation (mm) between 18 UTC 2 and 00 UTC 5 September 2004 and the best-track of Typhoon Songda (2004) from JTWC (http://metocph.nmci.navy.mil/jtwc). The TRMM 3B42 V6 3-hourly merged rainfall dataset, which was obtained from the Asia-Pacific Data-Research Center (APDRC) at University of Hawaii, was used. The same precipitation dataset was used as observed precipitation in Fig. 10 as well. The small box in D3 shows the interested area that will be used for area mean in Fig. 10.

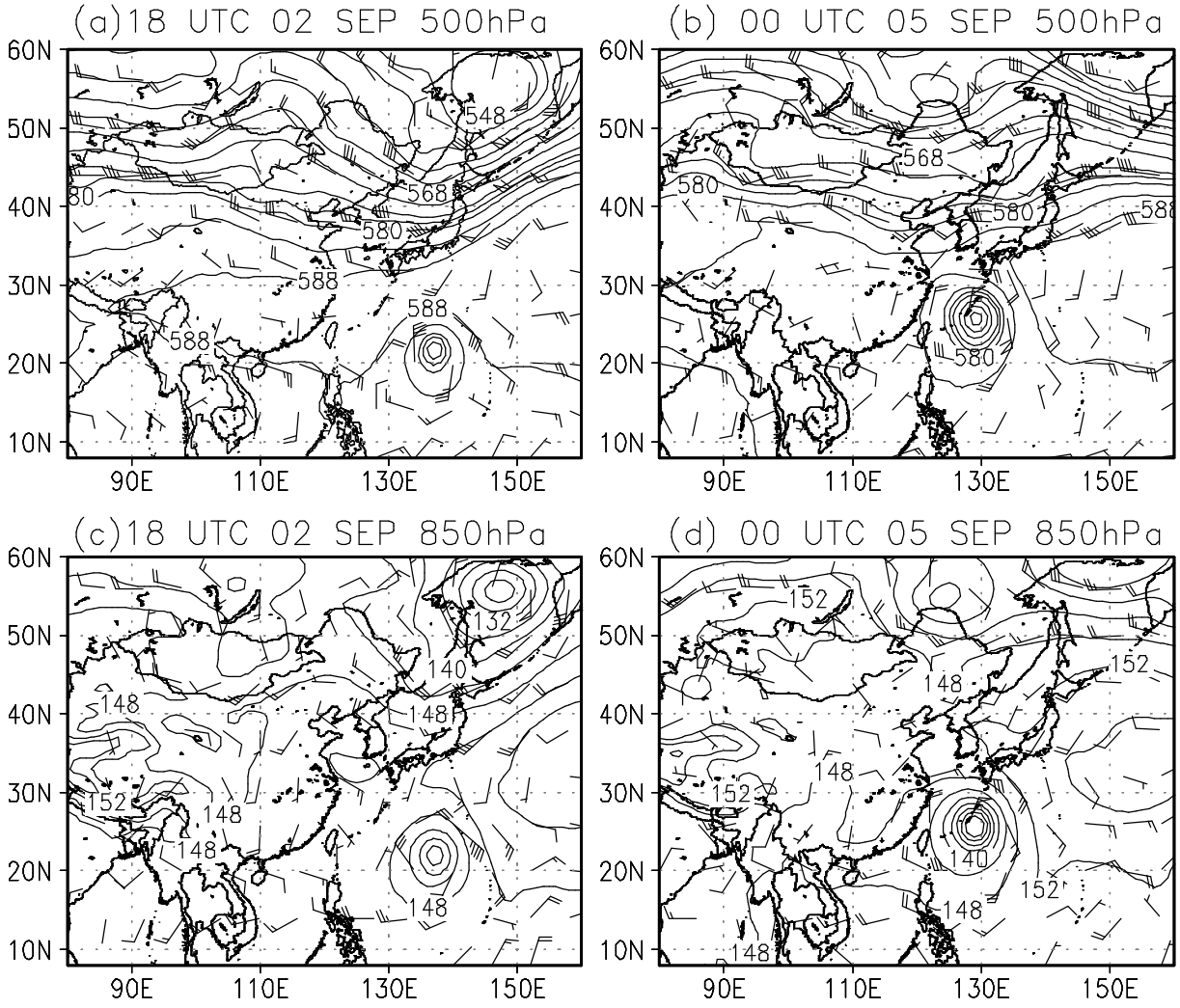

Fig. 2. Geopotential height (10 gpm in contours) and wind (wind barbs) fields at 500 hPa (upper) and 850 hPa (lower) with contour interval of 40 gpm from the FNL analysis for 18 UTC 2 (left panels) and 00 UTC 5 September 2004 (right panels). One flag represents 50 knots and one full barb represents 10 knots.

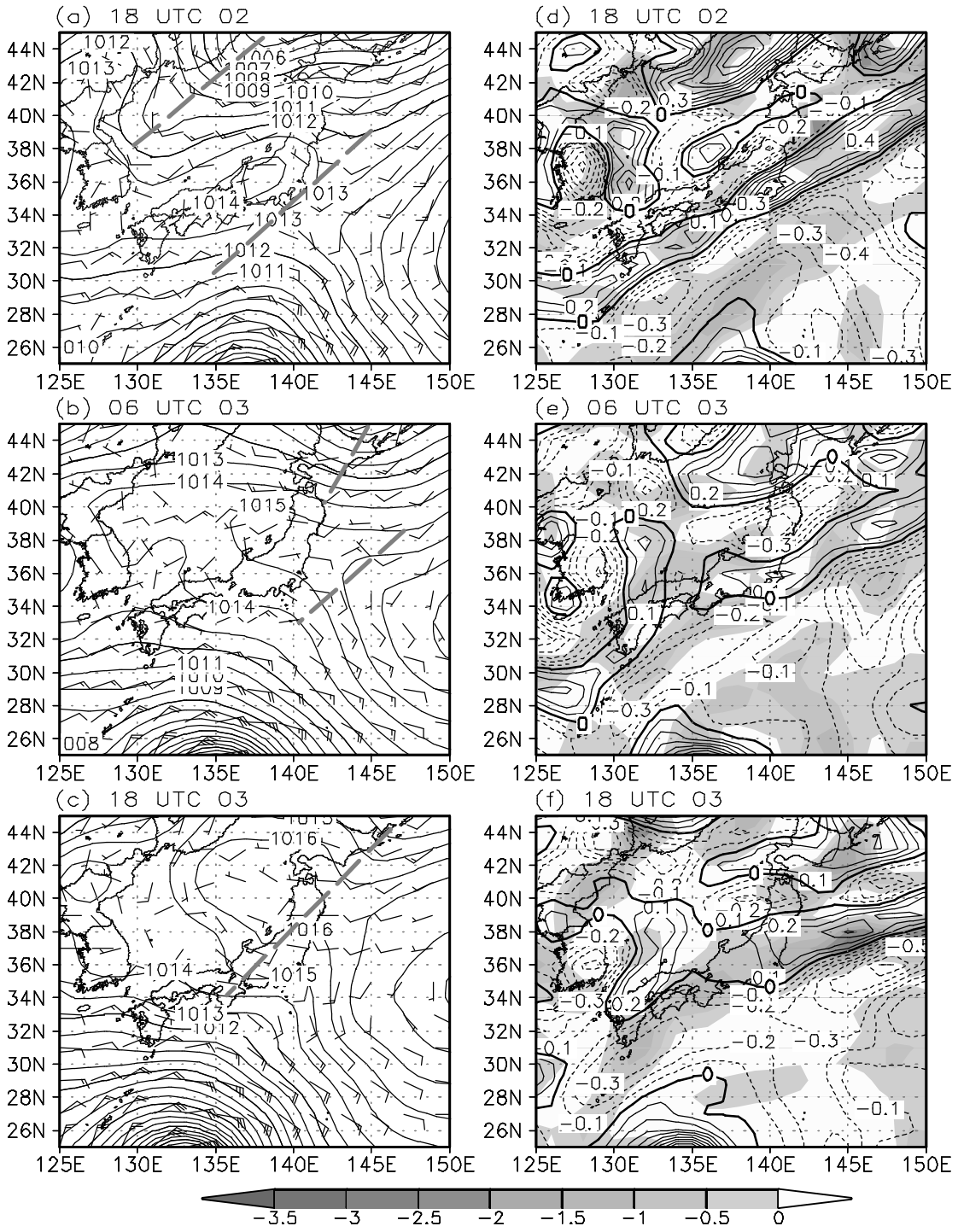

Fig. 3. 10-m wind (wind bars in m s^{-1}) and sea level pressure (contours with interval of 1 hPa) fields (left) and the horizontal divergence (shading in 10^{-5} s^{-1}) and relative vertical vorticity (contours with interval of 0.1×10^{-4} s^{-1}) at 18 UTC 2 (a and d), 06 UTC 3 (b and e), and 18 UTC 3 (c and f) September, 2004 from FNL analysis. One flag represents 50 knots and one full barb represents 10 knots. Thick Dashed line segments in (a)-(c) show either a short wave trough in the mid-latitude westerlies or a cyclonic shear line in the surface wind fields.

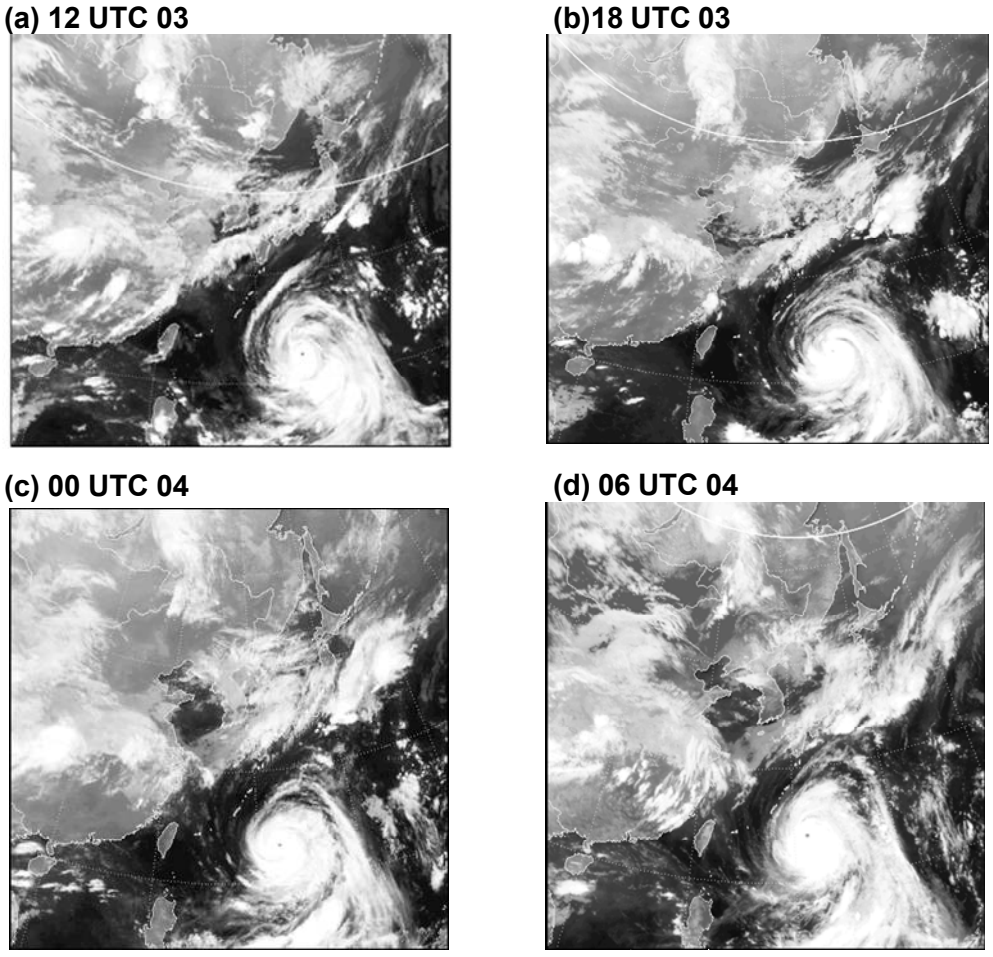

Fig. 4. Satellite images over the East Asia and western North Pacific (obtained from Korean Meteorological Administration), showing the evolution of Typhoon Songda (2004) and the precipitation system over the southern central Japan and adjacent seas with the time given at the top of each panels.

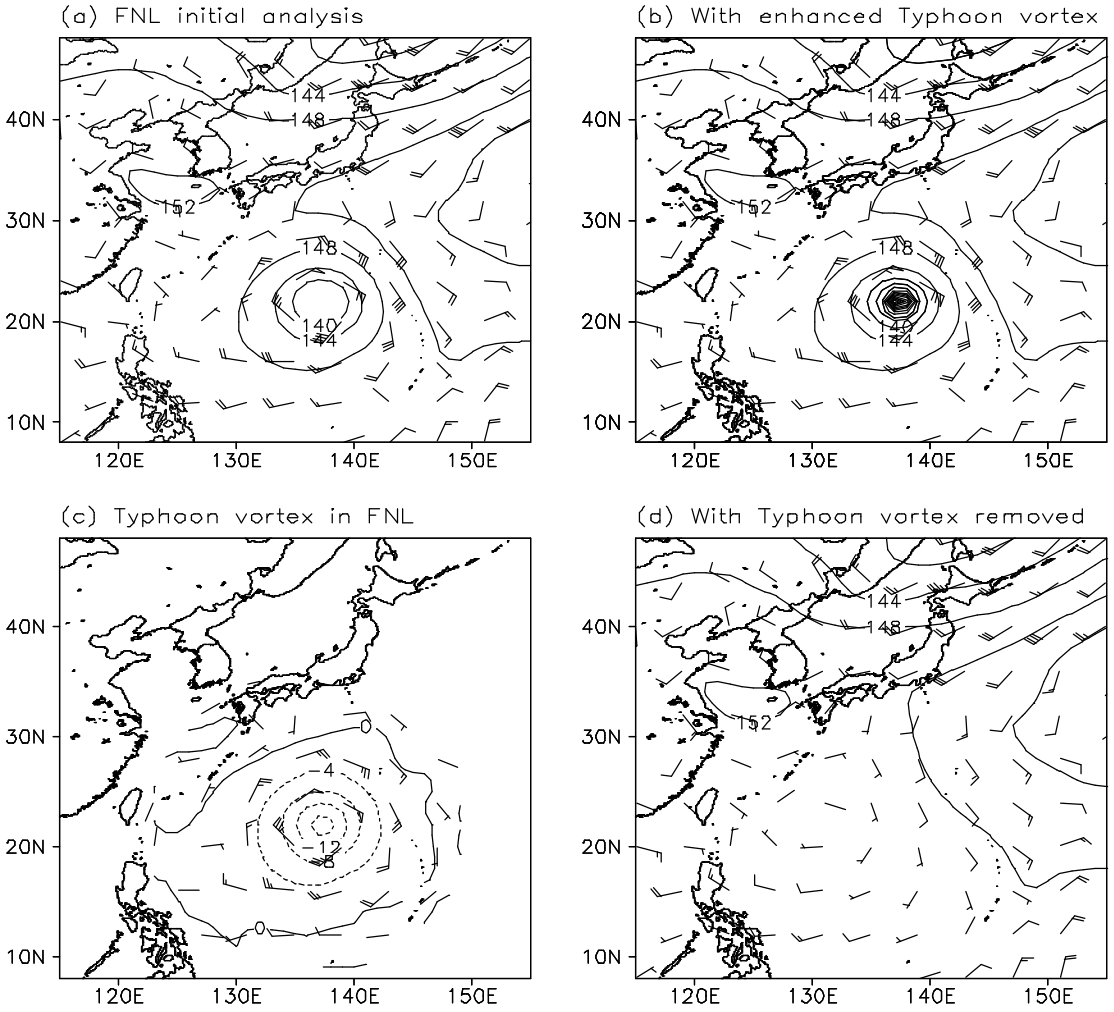

Fig. 5. Geopotential height (contours in 10 gpm with contour interval of 40 gpm) and wind (wind barbs) fields at 850 hPa 18 UTC 2 September 2004. (a) The FNL analysis; (b) initial condition in the control experiment with the enhanced typhoon vortex in the FNL analysis using a bogus vortex scheme; (c) the typhoon vortex removed from the FNL analysis; and (d) The initial condition in the No-Typhoon experiment with the typhoon vortex removed. One flag represents 50 knots and one full barb represents 10 knots.

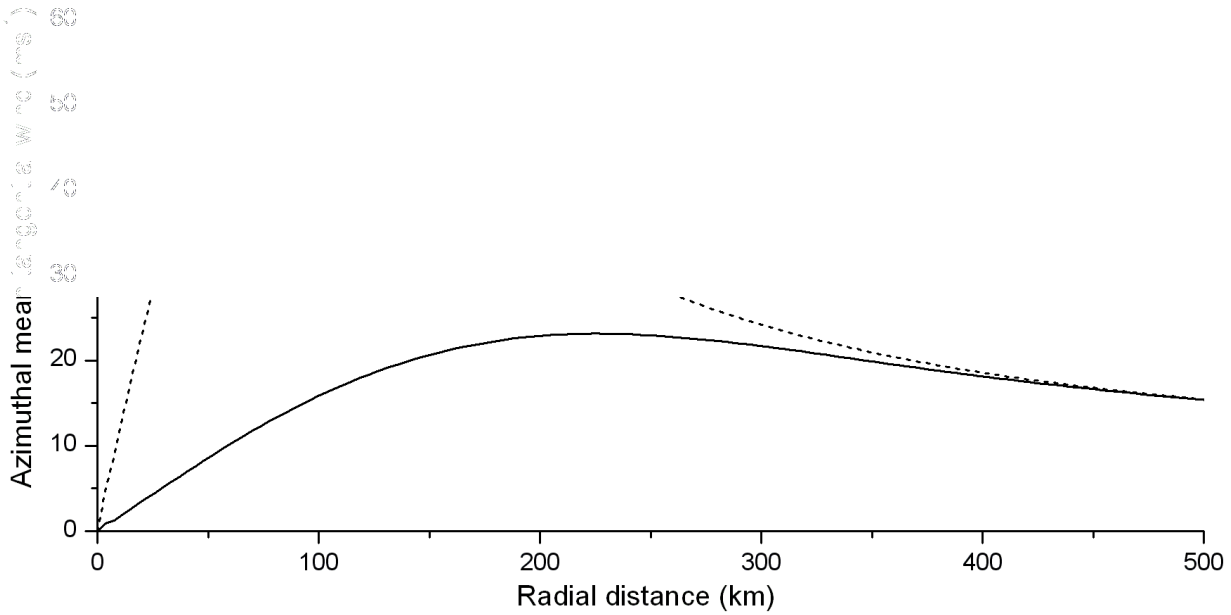

Fig. 6. Radial profiles of azimuthal mean tangential wind (m s^{-1}) at 850 hPa in the control experiment with a vortex bogus scheme (dashed) and in the No-Bogus experiment with no bogus vortex (solid) at the initial time (18 UTC 2 September 2004).

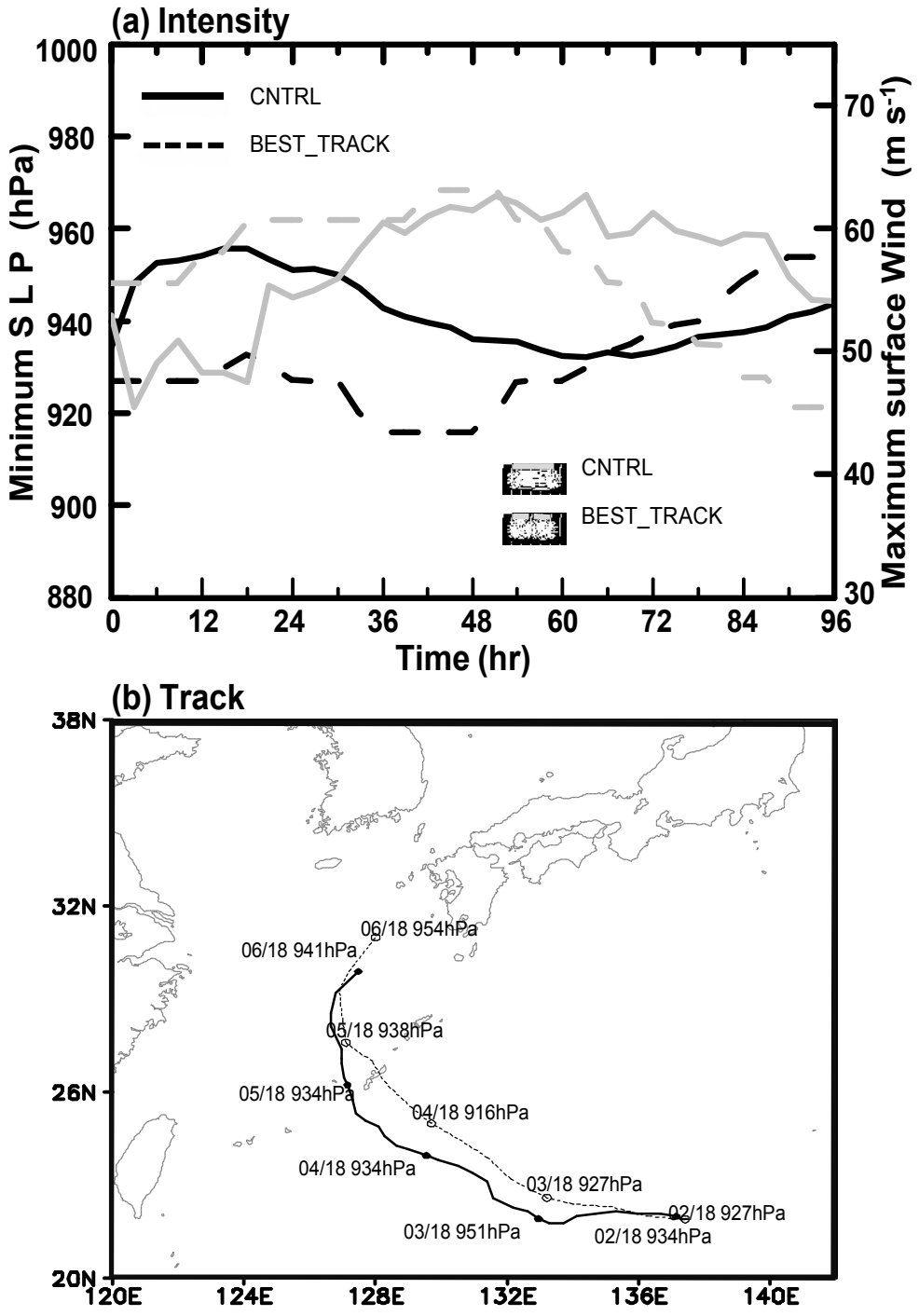

Fig. 7. (a) Evolution of the minimum central sea level pressure (hPa, left legend) and the maximum sustained 10-m wind speed (m s^{-1} right legend); and (b) the storm track from the JTWC best track data (dashed) and the WRF model simulation in the control experiment (solid).

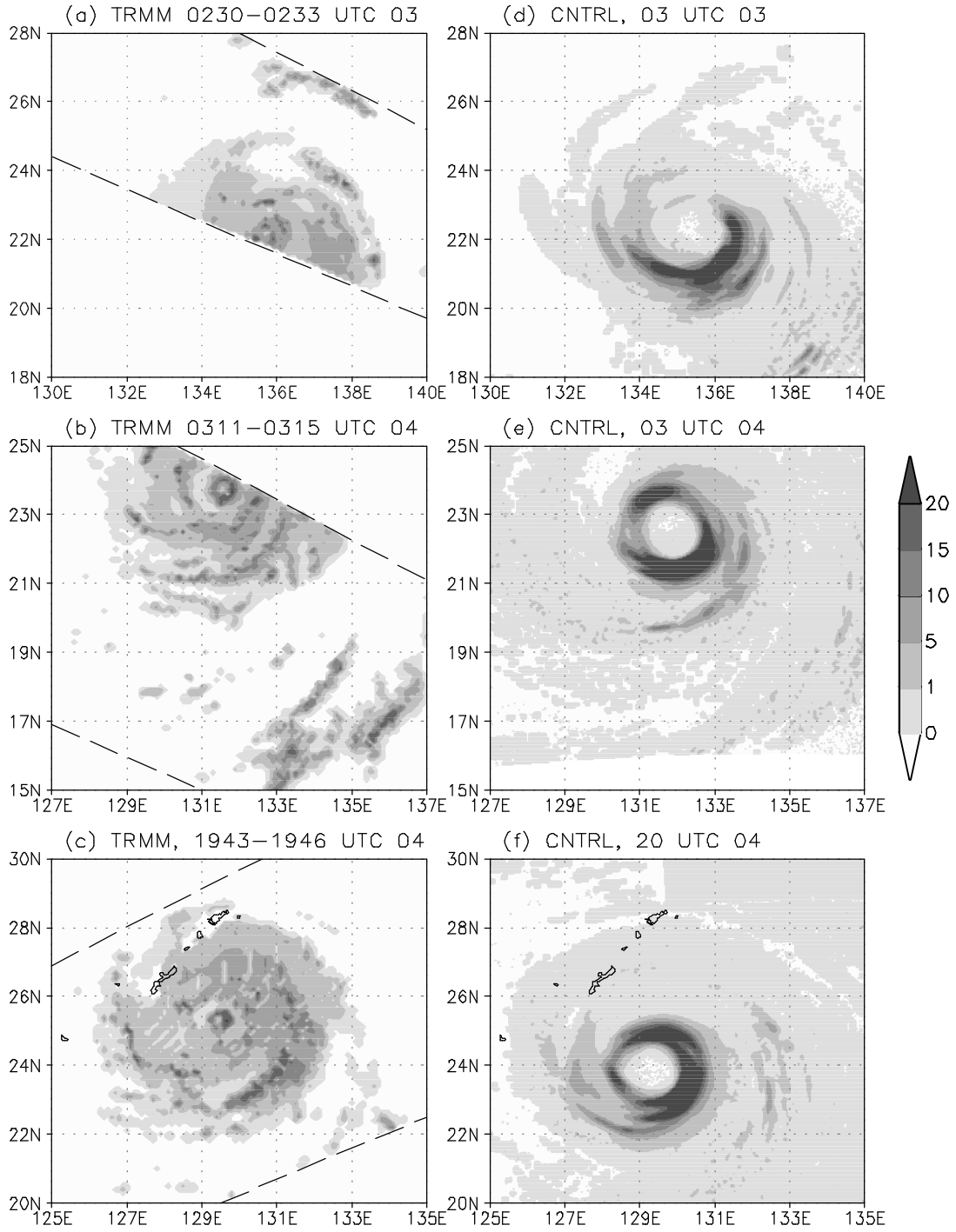

Fig. 8. Precipitation rates (mm h^{-1}) from the TRMM PR data (left) at 02:29:50-02:33:09 UTC 3 (top), 03:11:24-03:14:53 UTC 4 (middle), and 19:42:46-19:46:05 UTC 4 (bottom) September 2004; and from the control experiment (right) at 03 UTC 3 (top), 03 UTC 4 (middle), and 20 UTC 4 (bottom) September 2004.

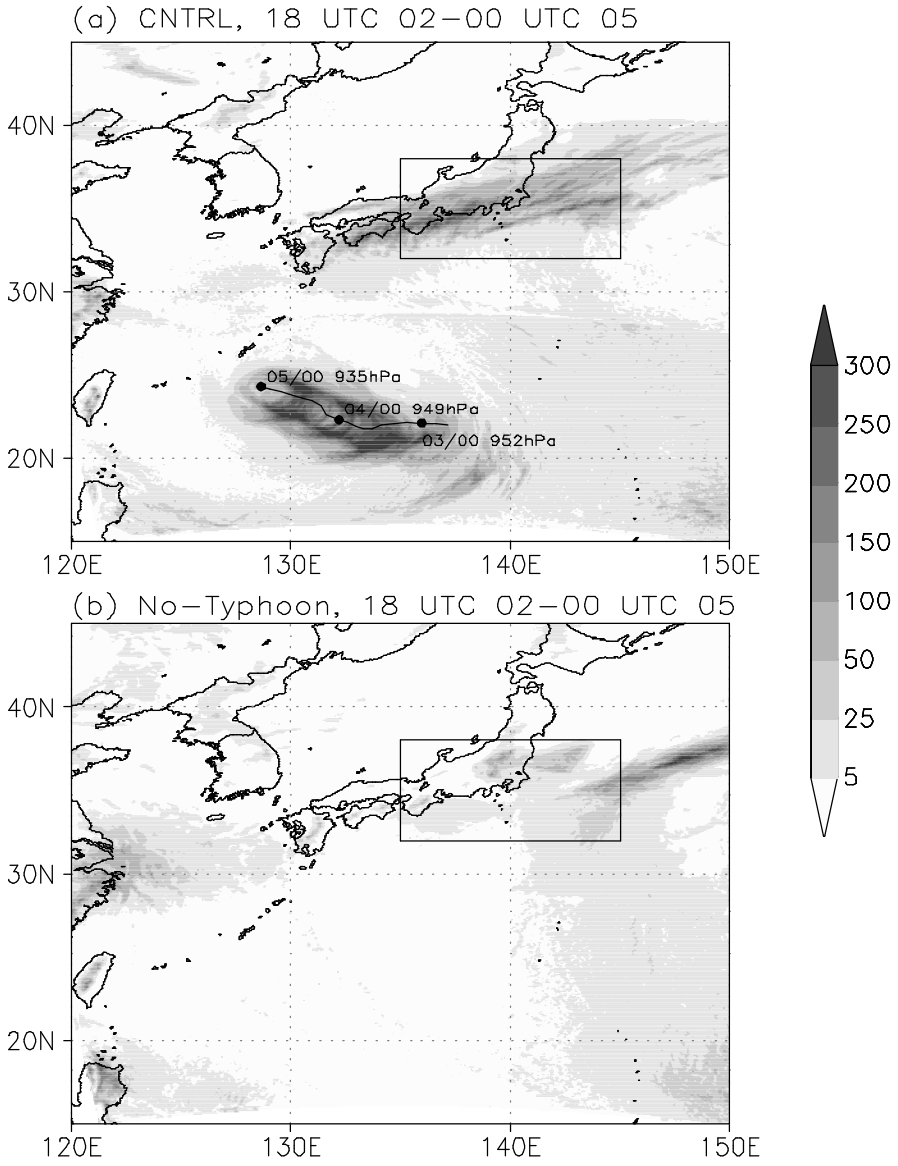

Fig. 9. Total precipitation (mm) between 18 UTC 2 September and 00 UTC 5 September 2004 in (a) the control experiment and (b) the No-Typhoon experiment. The typhoon track during this time period together with the minimum central sea level pressure from the control experiment is also shown in (a). The small box in each panel shows the interested area, the same as in Fig. 1, that will be used for area mean in Figs. 10 and 14.

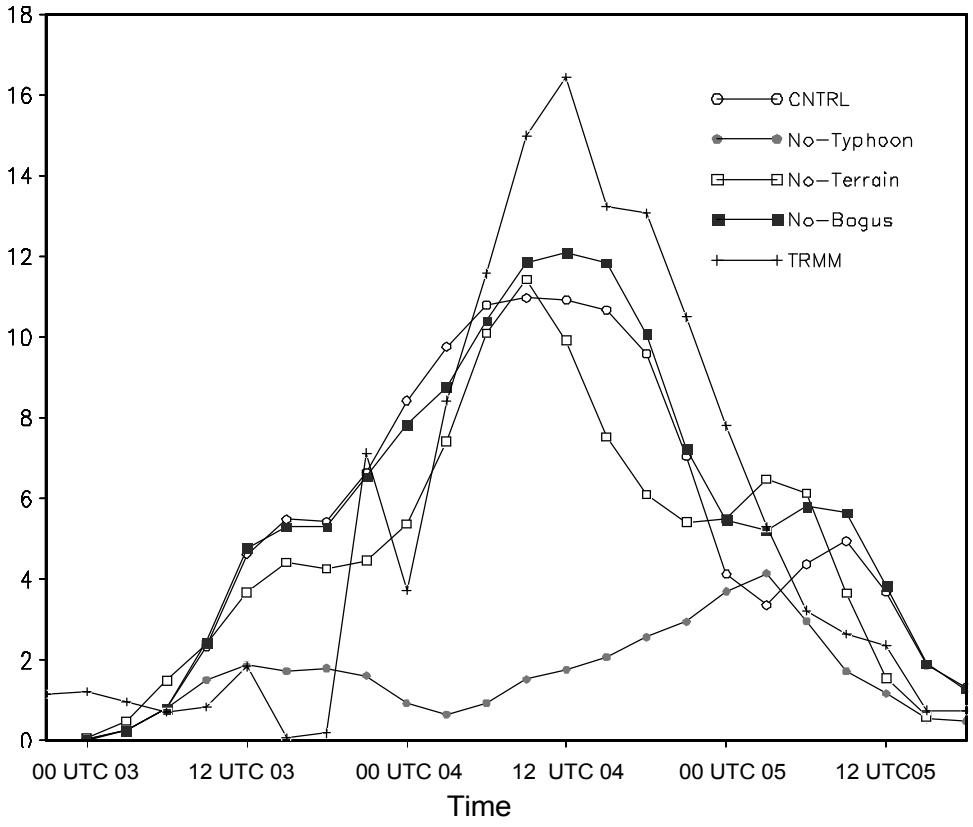

Fig. 10. Temporal evolution of 3-hourly rainfall (mm) from 21 UTC 2 to 18 UTC 5 September averaged in the area of 135°-145°E, 32°-38°N, namely, the box shown in Figs. 1 and 9, from the CNTRL, No-Typhoon, No-Terrain, No-Bogus experiment, and TRMM observation.

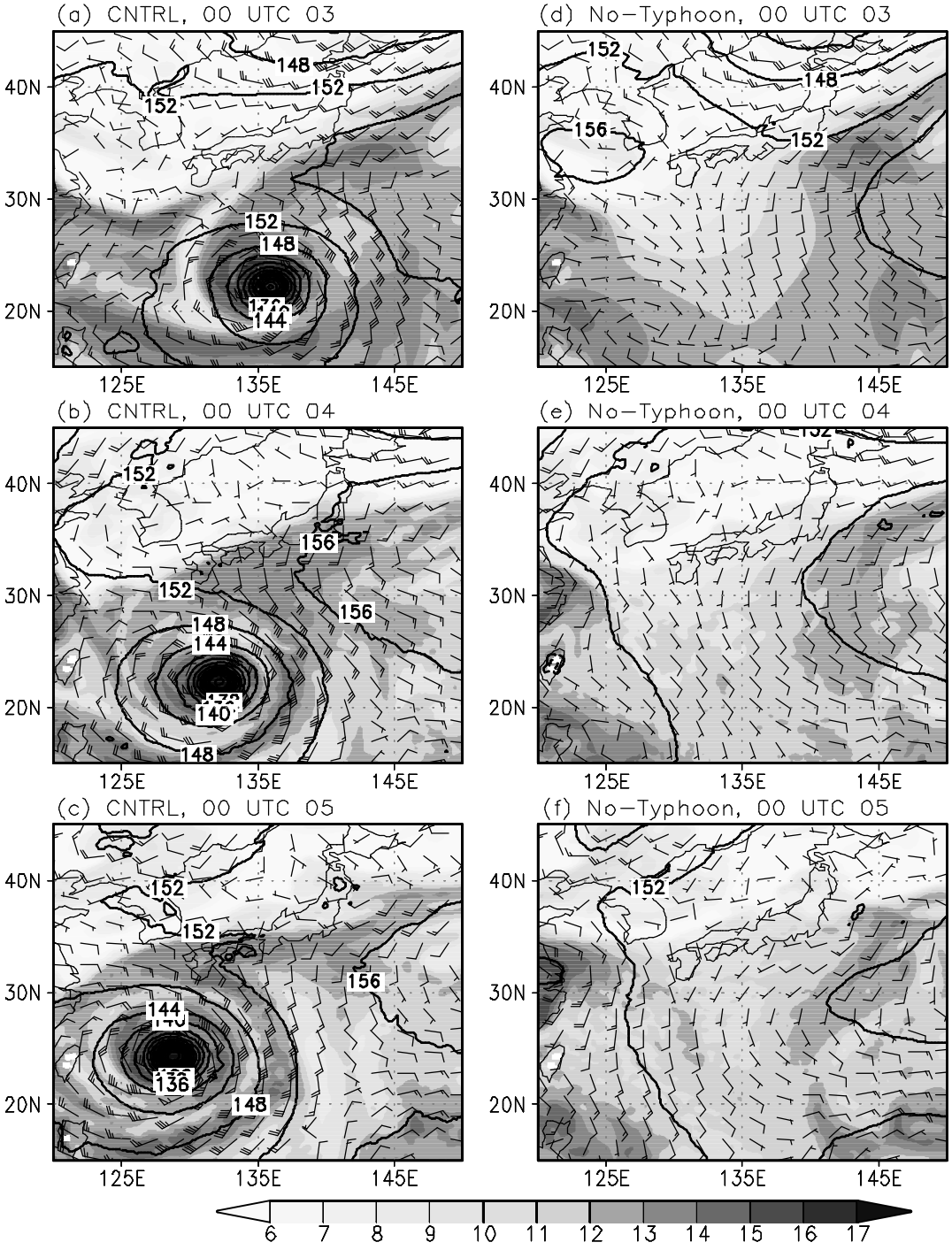

Fig. 11. Geopotential height (contours in 10 gpm with contour interval of 40 gpm), specific humidity (shading in g kg^{-1}), and wind (m s^{-1}, wind barbs) fields at 850 hPa from the control (left) and No-Typhoon (right) experiments, respectively, at 00 UTC 3 (top), 00 UTC 4 (middle), and 00 UTC 5 (bottom), September, 2004. One flag represents 50 knots and one full barb represents 10 knots.

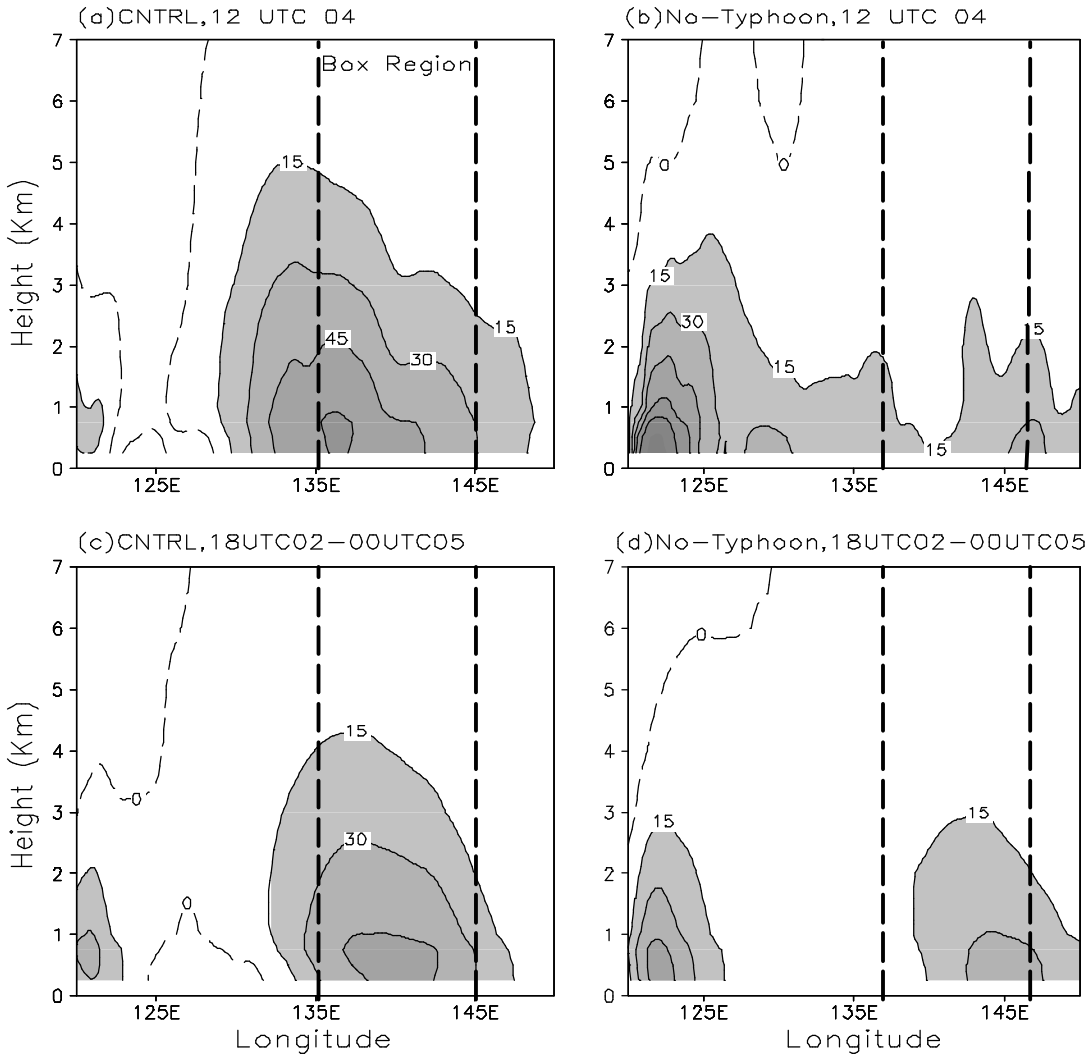

Fig. 12. Meridional moisture flux (10^3 g m^{-2} h^{-1}) across 30°N, (a) and (b) at 12 UTC 4 September 2004, (c) and (d) averaged between 18 UTC 2 and 00 UTC 5 September 2004. (a) and (c) from the control experiment, and (b) and (d) from the No-Typhoon experiment. Contour interval is 15×10^3 g m^{-2} h^{-1} and areas with values greater than 15×10^3 g m^{-2} h^{-1} are shaded. The longitude area of 135°-145°E for the box in Figs. 1 and 9 is marked with vertical dashed lines.

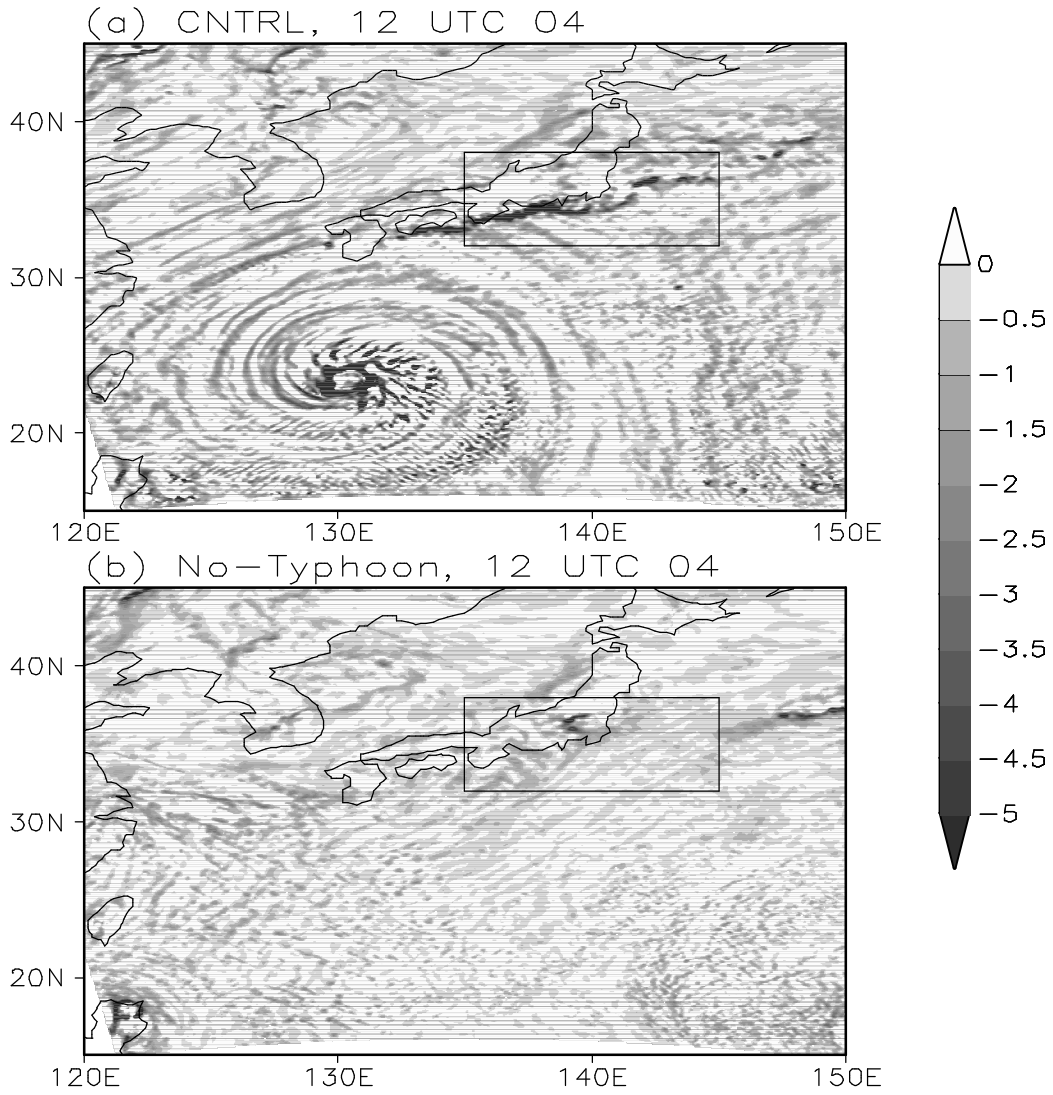

Fig. 13. Column-integrated moisture flux divergence (10^3 g m^{-2} h^{-1}) at 12 UTC 4 September 2004 from (a) the control experiment and (b) the No-Typhoon experiment.

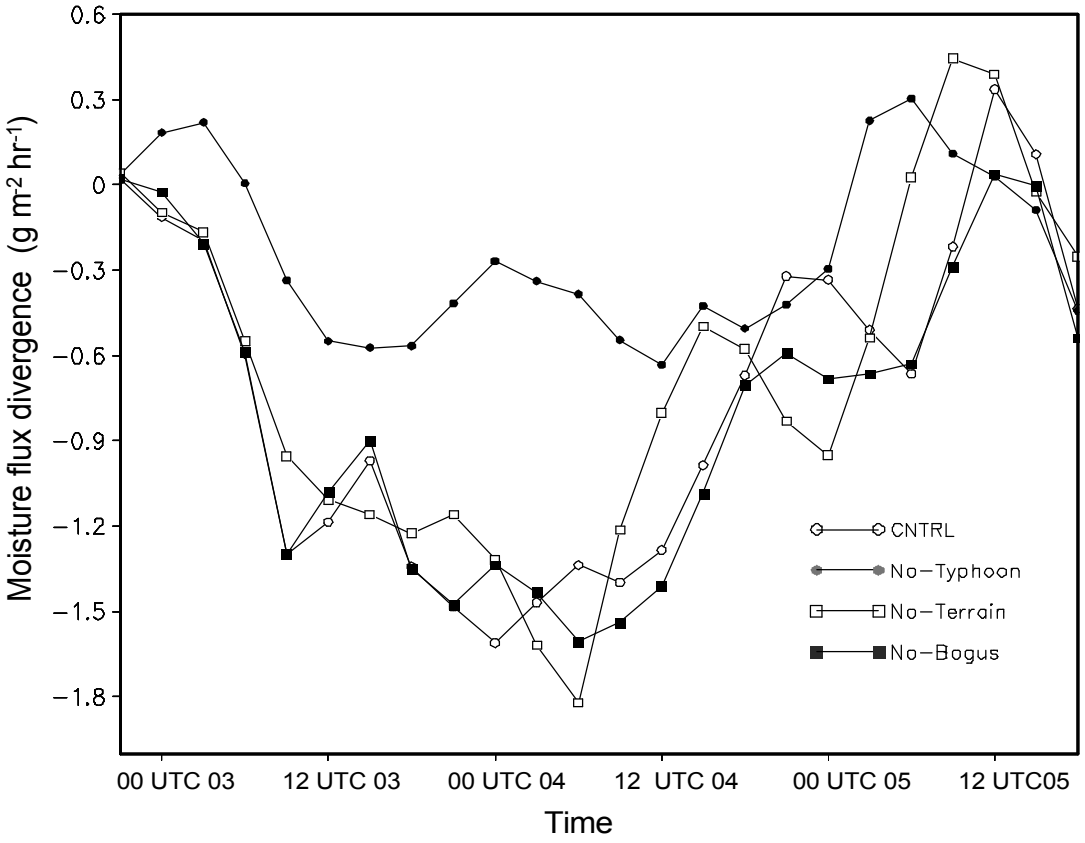

Fig. 14. The temporal evolution of the moisture flux divergence (10^3 g m^{-2} h^{-1}) averaged in the box given in Fig. 9 during 21 UTC 2 and 18 UTC 5 September 2004 from the control, No-Typhoon, No-Terrain, and No-Bogus experiments.

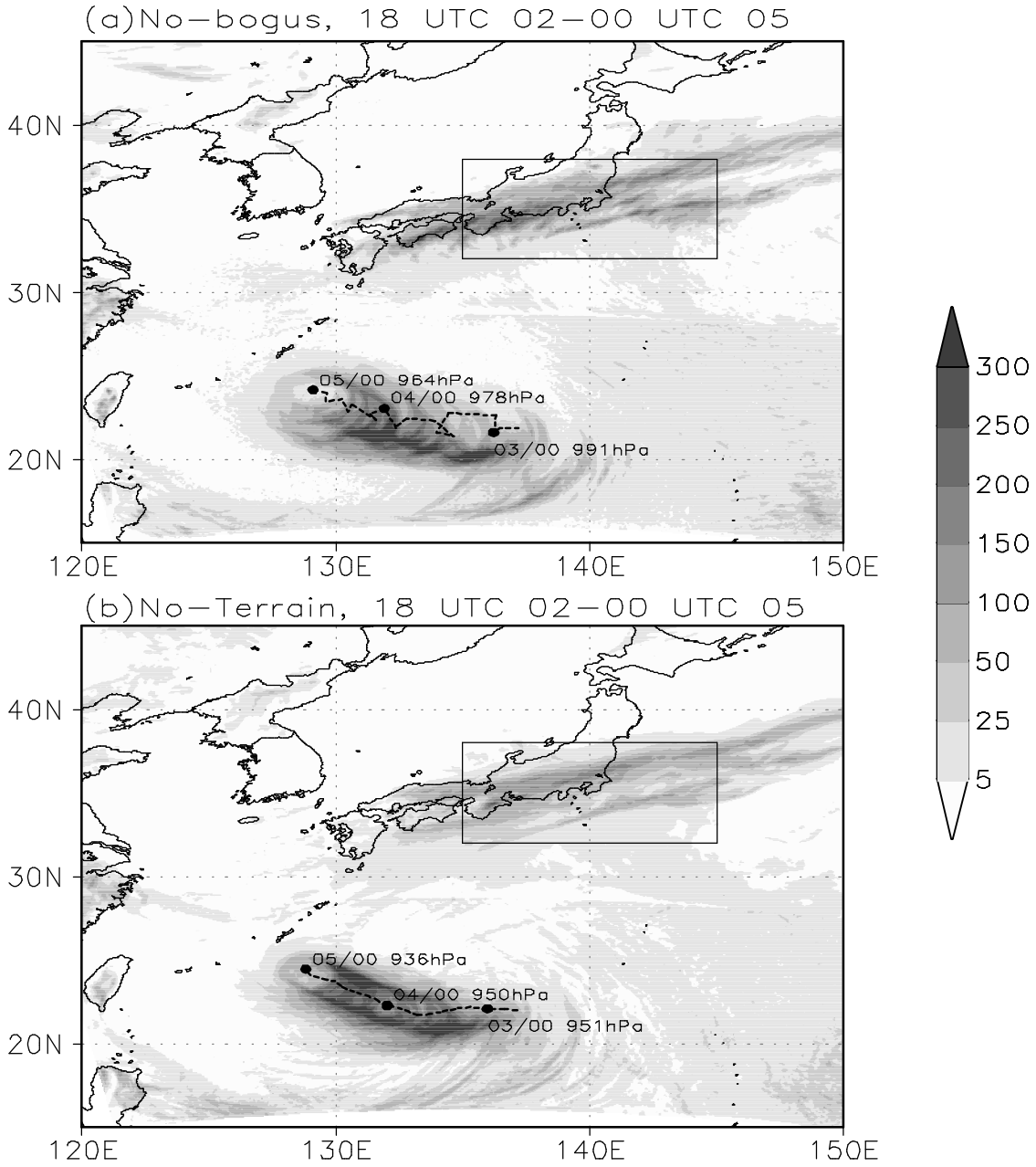

Fig. 15. Same as Fig. 9 but for (a) the No-Bogus experiment and (b) the No-Terrain experiment.